

Copyright 2007 Society of Photo-Optical Instrumentation Engineers.

This paper was published in Proceedings of SPIE, volume 6514, Medical Imaging 2007: Computer Aided Diagnosis and is made available as an electronic reprint with permission of SPIE. One print or electronic copy may be made for personal use only. Systematic or multiple reproduction, distribution to multiple locations via electronic or other means, duplication of any material in this paper for a fee or for commercial purposes, or modification of the content of the paper are prohibited.

Automated volumetric segmentation method for growth consistency of nonsolid pulmonary nodules in high-resolution CT

William A. Browder^a and Anthony P. Reeves^a and Tatiyana V. Apananosovich^b
and Matthew D. Cham^c and David F. Yankelevitz^c and Claudia I. Henschke^c

^aSchool of Electrical and Computer Engineering, Cornell University, Ithaca, NY;

^bSchool of Operations Research and Information Engineering, Cornell University, Ithaca, NY;

^cDepartment of Radiology, Weill Medical College of Cornell University, New York, NY

ABSTRACT

There is widespread clinical interest in the study of pulmonary nodules for early diagnosis of lung cancer. These nodules can be broadly classified into one of three types, solid, nonsolid and part-solid. Solid nodules have been extensively studied, while little research has focused on the characterization of nonsolid and part-solid nodules. Nonsolid nodules have an appearance in high-resolution CT consisting of voxels only slightly more dense than that of the surrounding lung parenchyma. For the solid nodule, robust techniques are available to estimate growth rate and this is commonly used to distinguish benign from malignant. For the nonsolid types, these techniques are less well developed. In this research, we propose an automated volumetric segmentation method for nonsolid nodules that accurately determines a nonsolid nodules growth rate. Our method starts with an initial noise-filtering stage in the parenchyma region. Each voxel is then classified into one of three tissue types; lung parenchyma, nonsolid and solid. Removal of vessel attachments to the lesion is achieved with the use of a filter that focuses on vessel characteristics. Our results indicate that the automated method is more consistent than the radiologist with a median growth consistency of 1.87 compared to 3.12 for the radiologist on a database of 25 cases.

Keywords: Nonsolid nodules, nodule segmentation, computer-aided diagnosis

1. INTRODUCTION

In the United States, lung cancer causes more deaths than the next 4 major cancers combined. Early diagnosis through the study of pulmonary nodules is now a focus of intense medical research. Nodules can occur as one of three main types: solid, nonsolid and part-solid. Nonsolid pulmonary nodules are regions of translucent tissue (sometimes referred to as ground-glass opacity, or GGO) which do not have solid components other than vessels. Compared to the more commonly studied solid nodules, nonsolid nodules have ill-defined borders and can surround vascular structures. These difficulties make volumetric assessment challenging (see Figure 6 for an example nonsolid nodule). Growth rate measurement of lung nodules is one of the principle factors in determining a nodule's malignancy. Therefore, the objective of this research is the development of an automated volumetric segmentation method to establish a reliable growth rate calculation for nonsolid nodules. The growth consistency of nodule measurement can be defined when volume estimates are made from scans at 3 different times. This metric compares the automated segmentation results with the boundary markings of a radiologist. An automated method that could reliably perform this task would be very useful in characterizing these types of nodules.

Previous work in the area of nonsolid nodules has mainly focused on segmentation techniques, while little work has examined accuracy in more important clinical applications, such as growth rate calculation. Growth rate assessment is particularly important due to the lack of information regarding these potential cancers. K. Okada, et. al.¹ proposed an anisotropic Gaussian fitting method to determine volumetric size of both solid and nonsolid nodules. This work was primarily focused on determining location and spread of solid nodules, and

Further author information: (Send correspondence to William Browder)
E-mail: wab26@cornell.edu, Telephone: 1 607 255 2993

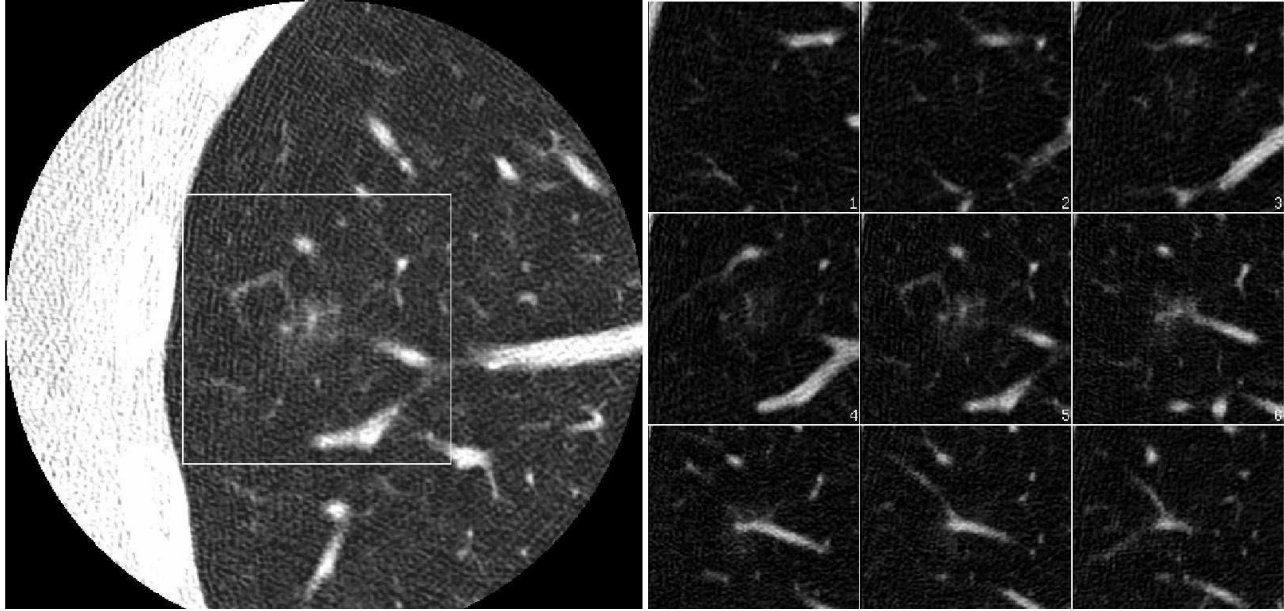


Figure 1. A nonsolid nodule in high resolution CT. The left image is a high-resolution clip indicating the ROI around the nodule. The image on the right is a montage of images containing the nodule.

only contained 10 nonsolid nodules out of a database of several hundred. Nonsolid component interacting with vessels are not specifically mentioned in their database (and is the most challenging case). Results were assessed by visual interpretation by an expert observer. L. Zhang, et. al.² developed a segmentation algorithm utilizing a markov-random field (MRF) model for the intensity distribution of the nodule. The results focused exclusively on the consistency of measurement from the automated segmentations on 25 nodules. There was no comparison of growth rate computation or segmentation accuracy.

Yoo, et. al.³ proposed a deformable model approach to define the boundary of the nonsolid nodule. This approach uses a level set method to classify the nodule into one of several regions in order to remove vascular structures. The level set procedure they used was on 2D slices of the 3D data and would require a higher order level set function to support a three-dimensional volumetric segmentation. Tachibana, et. al.⁴ developed a method for segmentation method for nonsolid nodules using a model based on the watershed method. A set of 23 cases provided by the LIDC were examined and the coincident rate between the radiologist marking and the automated segmentation result was reported. It was unclear how many of the nodules were nonsolid or solid nodules within the dataset. No results were reported on accuracy of growth rate computation.

2. METHODS

The automatic nonsolid nodule segmentation method is divided into several stages, as shown below in Figure 2. These stages include pre-processing, noise reduction, voxel classification and vessel removal.

2.1. Nonsolid Nodule Segmentation

The first step of our segmentation algorithm is to have the operator draw a line through the largest slice of the nodule. From this information we can determine the maximum extent and central point of the nodule. Once these have been determined, the region-of-interest (ROI) of the nodule is generated. This ROI is extracted to three times the size of the given maximum extent measurement to be sure to capture all the nodule region and the surrounding areas in all image slices. The region is then resampled from an anisotropic image resolution to an isotropic image space of 0.25 mm^3 voxels using super-sampling. An overview of this procedure is given in the paper by Kostis et. al.⁵ for the case of solid nodules.

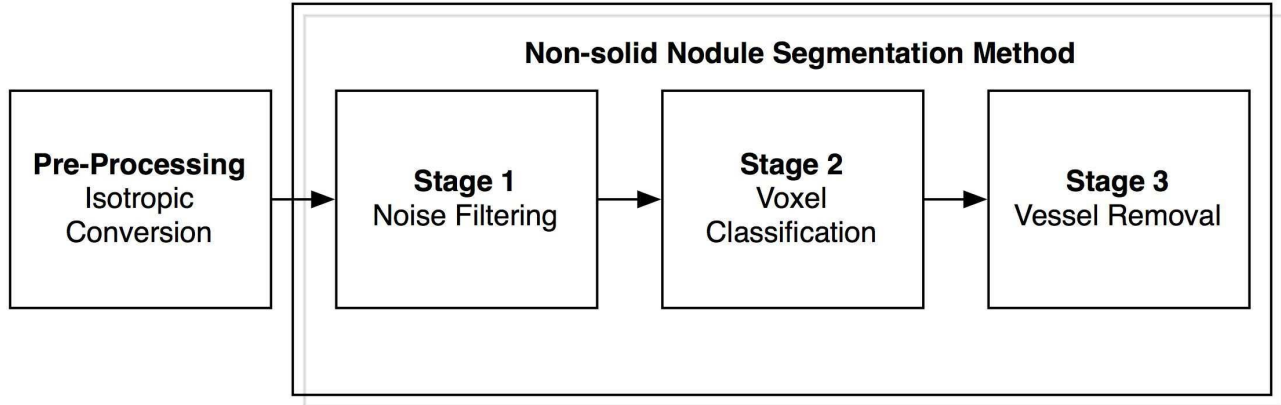


Figure 2. Flowchart of nonsolid segmentation method consisting of CT image pre-processing and three major stages.

2.1.1. Noise Filter

Noise occurring in the region of the nonsolid nodule can be particularly problematic if voxels are not classified correctly. The objective of the noise filter is to smooth the homogeneous regions in the nodule, while retaining as much edge information as possible. For noise filtering we used a bilateral filter method by Tomasi, et. al.⁶ which is described in equation 1.

$$I_{smooth}(x) = k_d^{-1}(x) \cdot \sum_{-\infty}^{\infty} f(n) \cdot c(n, x) \cdot s(f(n), f(x)) \quad (1)$$

The pixel location is denoted by x , whereas the n term denotes a neighbor w.r.t. x . The $k_d(x)$ term is the neighborhood kernel of the function and is used to normalize the results. The closeness function $c(n, x)$ (equation 2) is a weighting term based on the geometric proximity. The similarity function $s(f(n), f(x))$ (equation 3) is a weighting term based on intensity. Both the similarity and geometric closeness functions can be defined as gaussian functions of their euclidean distance.

$$c(n, x) = e^{-\frac{1}{2} \left(\frac{d(n, x)}{\theta_d} \right)^2} \quad d(n, x) = \|n - x\| \quad (2)$$

$$s(n, x) = e^{-\frac{1}{2} \left(\frac{a(f(n), f(x))}{\theta_r} \right)^2} \quad a(n, x) = \|n - x\| \quad (3)$$

In Tomasi's work, the parameters θ_r, θ_d were selected to be 30,10 respectively. These values were used in our filter and provided acceptable results.

2.1.2. Voxel Classifier

We propose a three-level voxel model for the segmentation of nonsolid nodules that incorporate the three tissue types that characterize the composition of these nodules. This three-class model consists of defining each voxel in the ROI as parenchyma, nonsolid or solid tissue types. Solid tissue commonly occur at intensity values greater than -474 HU (hounsfield units). These voxel types represent large vessels and the pleural surface. Nonsolid voxels are those with attenuation level slightly more than that of lung parenchyma, but significantly less than solid tissue. Lung parenchyma voxels are less dense and are considered a background class for the purposes of our segmentation technique.

Determining the appropriate values for the voxels within the ROI is particularly challenging. Some of the issues include distribution overlap between the parenchymal and nonsolid tissue classes and CT image noise.

Table 1. Three voxel classification types

Name	Intensity Range
Solid Voxel Tissue	Greater than about -474 HU
nonsolid Voxel Tissue	Typically between -474 HU and -804 HU
Parenchymal Tissue	Less than about -804 HU

The proposed solution to these issues is a probabilistic approach to the three-tissue classification model based on empirically determined intensity levels, τ_h for solid voxels and τ_{ns} for nonsolid voxels. The τ_h parameter was determined using an adaptive histogram technique outlined in Reeves, et. al.⁷ The τ_{ns} level was determined through examination of several scans and was set to a global value of -780 HU. Once the two intensity values τ_h and τ_{ns} have been determined, a gaussian probability curve is created at each intensity level (equation 4).

$$P(I(v)) = \frac{1}{\sqrt{2\pi}\sigma} e^{-\frac{v^2}{2\sigma^2}} \quad (4)$$

where $V = \tau_{ns} - I(v)$ and σ defines the standard deviation of the gaussian curve. The value of σ was chosen to be 10, based on the observed variance of several scans in the nonsolid voxel intensity range.

$$P_{voxel-class} = 0.5 \cdot P(I(v)) + 0.5 \cdot \sum_{k=0}^n N(k) \cdot P(I(v+k)) \quad (5)$$

Incorporation of neighborhood information during the classification stage can also reduce the impact of image noise in the parenchyma region classified as nonsolid voxels. In our probability function, equal weight was given to intensity and neighborhood information, as in Equation 5, where $N(k)$ represents the three-dimensional 6-way connected neighborhood.

2.1.3. Vessel Removal

A challenge in effective nonsolid nodule segmentation is the removal of vascular connections to the nodule. This is difficult for two reasons; a) smaller vessels occur with a similar intensity pattern making them often classified as nonsolid and, b) vessels frequently intersect nonsolid nodules (nearly 80% of the cases in our database). Removing such vessels while retaining the original shape of the nodule is the objective of the vessel removal filter.

There has been some work in the area of restricted morphological processing,⁸ which only erodes/dilates pixels with specific features, typically volume occupancy within the kernel. Our proposed vessel filter builds on this work by including structural information of the binary objects. This filter consists of a series of stages, designed to isolate the nodule from the pleural surface, vessels connected at the periphery of the nodule and vessels within the nodule.

The first stage of the filter removes all voxels classified as solid tissue. This removes a majority of the pleural surface, part-solid voxels occurring within the center of vessels and solid component within the nodule. The next two stages of the algorithm repeat for all nonsolid classified voxels within the ROI. An ellipsoid kernel was chosen to better reflect the anisotropic nature of the original image data (specifically, the lower axial resolution). The sizing of the kernels was determined as a function of the nodule size (provided as an input from the investigators two-click method) in equation 6.

$$V_s = \frac{N_s}{2} + 1 \quad (6)$$

For all sizes while $N_s > 1$. The first stage of the vessel removal algorithm examines the number of nonsolid voxels found within the specified kernel. A parameter, θ_r is a restrictive parameter that is a voxel occupancy sizing criteria. If the occupancy percentage within the kernel is greater than that of the θ_r than the voxel is

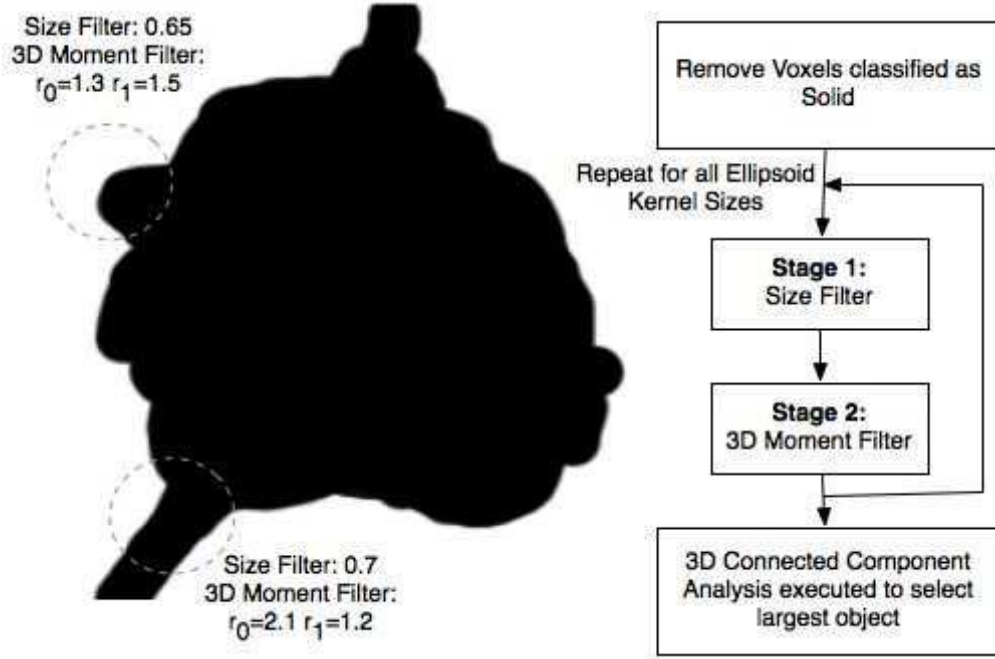


Figure 3. Diagram and flowchart outlining the operation of the vessel removal filter

passed onto the next stage of processing. Based on a cylindrical vessel model, the θ_r parameter was chosen to be 0.5, representative of the percentage of volume a cylinder would occupy within the ellipsoid kernel.

The second stage filter examines the structural significance of the ROI. Using three-dimensional moment analysis on the nonsolid voxel binary image, we can determine the first and second order moments and construct the ellipsoid of inertia about the ROI. Examination of the calculated eigenvalues can reveal the nature of the structure of the binary region. We define the three eigenvalues describing the principle axes of the binary object as $\lambda_0, \lambda_1, \lambda_2$ in order of decreasing magnitude. Our approach models vessels as being similar to cylinders structurally and we can examine the ratios in equation 7. In the case of cylindrical vessels, we expect r_0 to be significantly higher valued and r_1 to be near 1.0. Removing only voxels with eigenvalue ratios within a tolerance can retain a larger percentage of the original nodule's shape.

$$r_0 = \frac{\lambda_0}{\lambda_1} \quad r_1 = \frac{\lambda_1}{\lambda_2} \quad (7)$$

The final stage of the filter a three-dimensional connected component filter designed to remove vessels and other structures that have been disconnected from the nodule. The result of the vessel removal filter is shown in Figure 4.

2.2. Growth Consistency

Growth rate computation is an important clinical parameter in deciding whether an indeterminate nodule is malignant. One of the principle goals of this research is to determine a confidence metric for measuring growth rate consistency between a radiologist and our automated method. To accomplish this task, we need to measure nodule volume at three different time points, so as to calculate two consecutive growth rates. We define a nodules growth rate using an exponential model and the doubling time (in days) is given below in equation 8.

$$DT = \frac{\ln 2 * \Delta t}{\ln(V_2/V_1)} \quad (8)$$

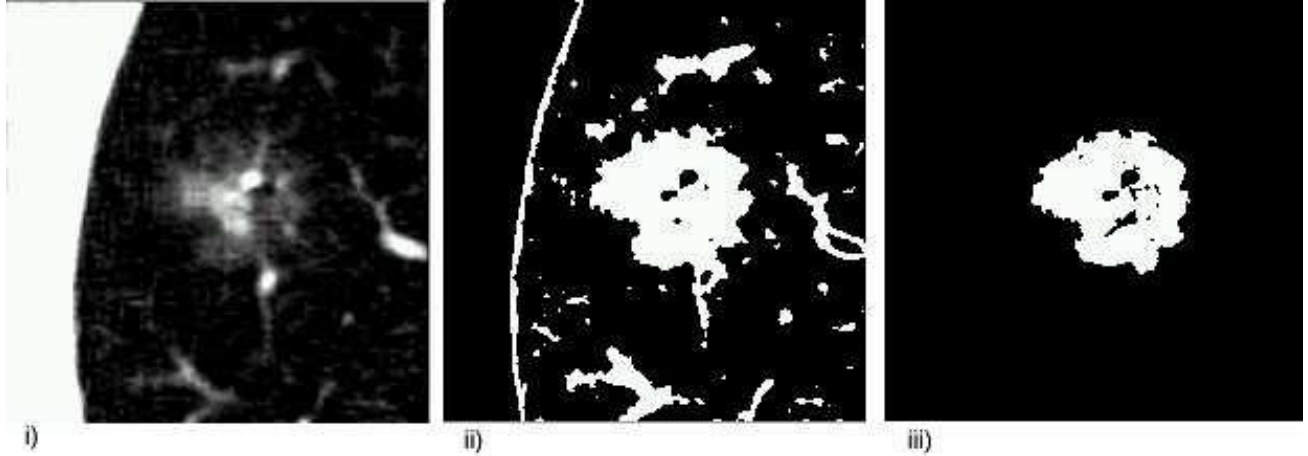


Figure 4. Image i) on the left is the windowed input CT image. Image ii) is the nonsolid classified voxels. Image iii) is the same image after the vessel removal filter.

where V_1, V_2 are the nodule volumes separated by Δt . Significantly lower DT values are commonly associated with malignant nodules. Nodule growth per month can also be defined. The growth index (GI) of a nodule is the percent change in volume per month and is defined below in equation 9. The GI metric is useful in the comparing growth rates over a short amount of time.

$$GI = 100 * 2^{((30.44/DT)-1)} \quad (9)$$

Growth consistency can be determined by examining consecutive growth rates over a set of three distinct time scans of a single nodule. The first growth rate calculation can be compared with the second and the difference can be a measurement of consistency. The growth consistency value is defined below:

$$GC = |GI_1 - GI_2| \quad (10)$$

In the ideal case, nodule growth consistency should be 0.0, or no difference between the two growth rates. Lower growth consistency values increase the confidence in our growth metric, whereas higher values can be a measurement of error in percent volume per month.

3. DATASET

The CT dataset for the evaluation of our algorithm consisted of 75 scans from the ELCAP project. Cases were selected randomly with the only requirement being three or more sequential scans existing of the same nonsolid nodule. Due to the longer time intervals between the scans, several of the scans were of differing resolutions depending on the year and technology deployed at the screening center. The resolution information is included in table 2.

Table 2. Number of scans at specific resolutions (25 nodules for 75 total scans)

	$\sim 0.6\text{mm} \times 1.25\text{mm}$	$\sim 0.6\text{mm} \times 2.5\text{mm}$	$\sim 0.18\text{mm} \times 1.00\text{mm}$
Number of Cases	50	10	15
Scan Type	Whole Lung	Whole Lung	Targeted Scan

The scans were generated on either a GE Medical Systems Lightspeed Ultra scanner (58 scans) or a GE Medical Systems QX/i scanner (17 scans). Each case has the same nodule at three different scan dates. A

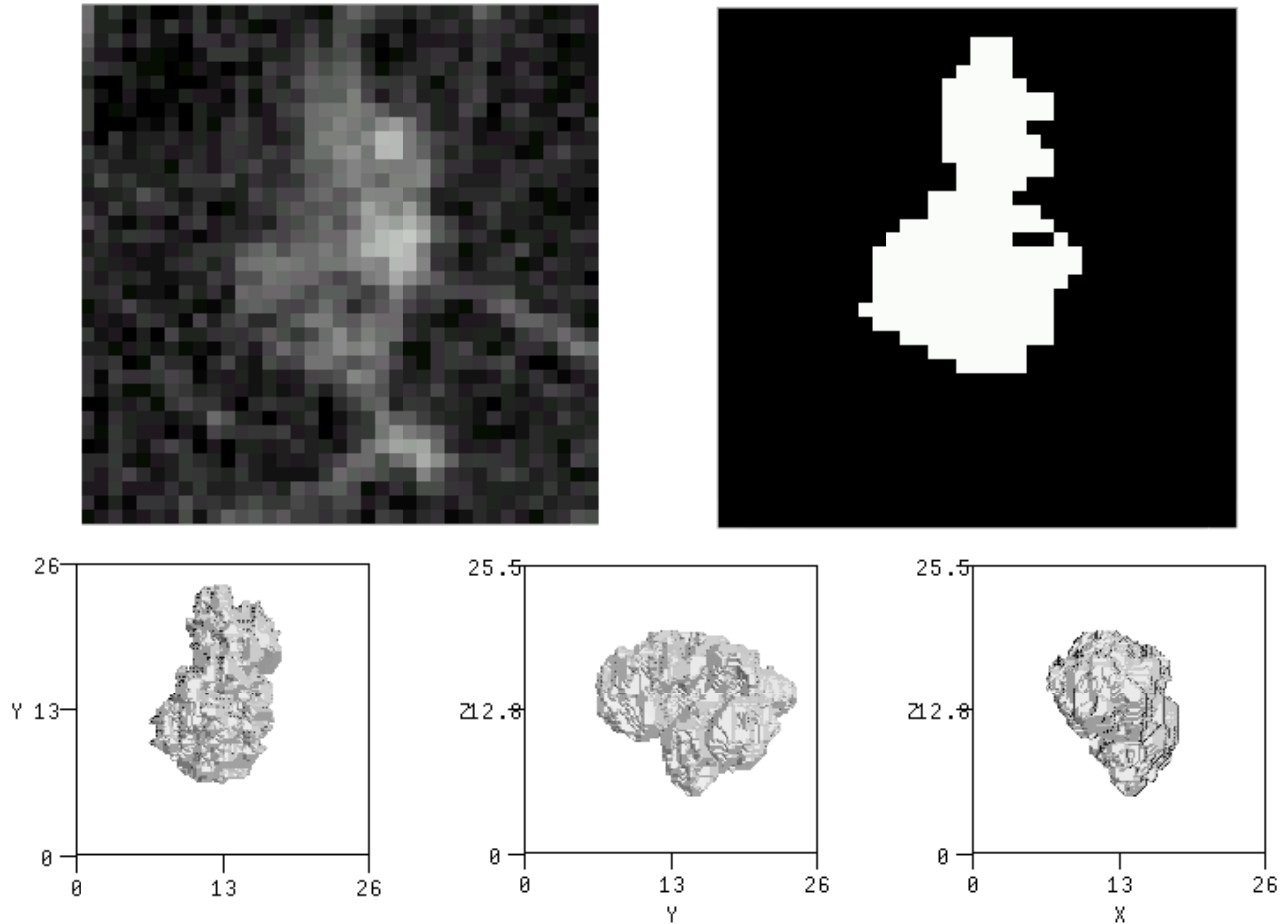


Figure 5. An example nonsolid nodule segmentation. The upper left image is the largest slice CT image of the nodule. The binary segmentation result is in the upper right image. The bottom image is the three-dimensional model of the nodule shown in axial, sagittal and coronal views.

radiologist examined the nodule at each time scan for the case. All slices of the image that contained the nodule were outlined by the radiologist to form a boundary. These boundary markings were then converted into a volumetric reading for comparison with our automated results.

The diameter of the nodules ranged from 5.6 mm to 17.5 mm with a median of 9.9 mm. The size information is included in Figure 7. Most of the nodules in our dataset are of sizes 8-15 mm in diameter at their largest slice. Nodules smaller than 8 mm are difficult to identify for a radiologist, commonly being confused with noise and other imaging artifacts.

The scan interval time is important in assessing the accuracy of growth-related calculations. A longer time interval is less susceptible to noise in size measurements, a common problem with smaller size nodules. Shortened time intervals may overestimate the growth rate and lead to erroneous clinical conclusions. In order to reduce this effect, cases with less than 100 day intervals between scans were not considered. The median interval time between scans was 347 days.

4. RESULTS

The growth consistency experiment design consisted of comparing growth rate calculation between our automated method and that of an expert radiologist. The GC metric (as defined in equation 2) was used to compare the

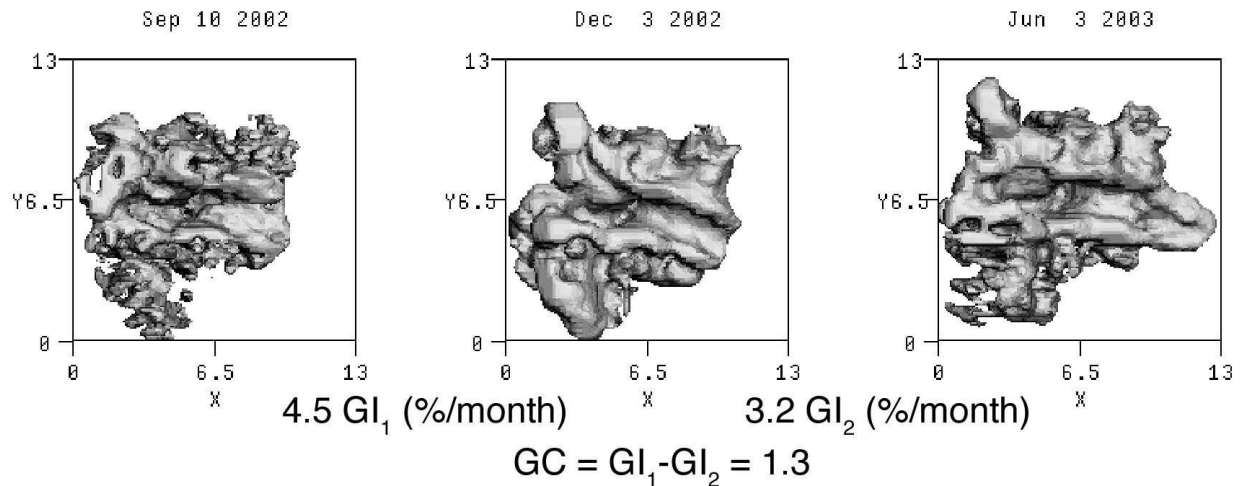


Figure 6. An example nodule that is growing at a rate of 4.5% volume per month during the interval between the first two scans. The second growth rate calculation between the second and third scans is 3.2 % volume per month. The difference between the two growth calculations gives us our consistency metric of 1.3.

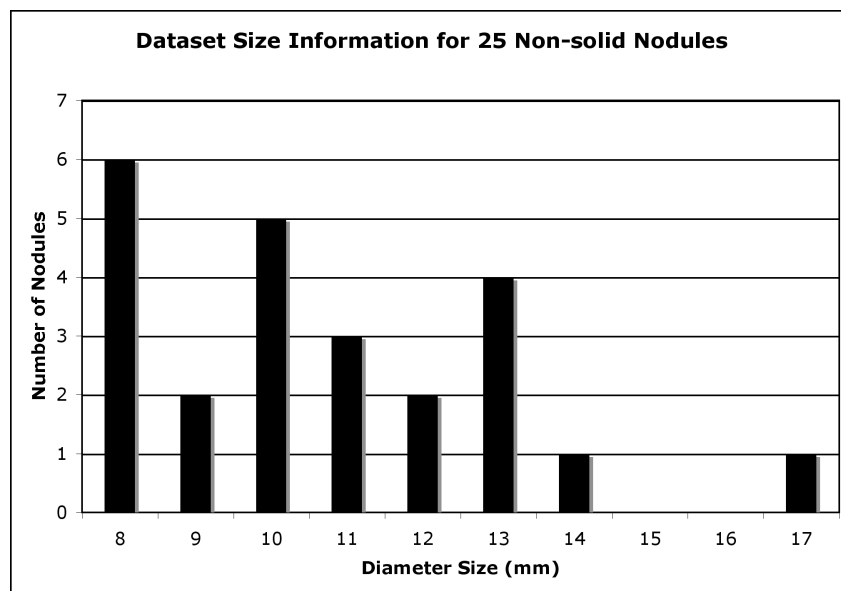


Figure 7. Dataset size information for set of 25 nonsolid nodules. The size is diameter(mm) and is the average size over the three time scans. The median size was 10.5 mm and the mean was 11.0 mm.

growth consistency of 25 cases. A total of 75 segmentations were computed using our automated method as well as 75 3D boundary markings outlined by a radiologist.

The results are reported in table 3. The median GC metric for the automated method is significantly lower than that of the radiologist. In fact, in 20 out of 25 (80 %) of the cases examined the automated segmentation technique was found to be more consistent than the radiologist (lower error in growth calculation). Our method exploits the power of the automated technique to deliver more consistently stable results when computing growth rates of lung nodules. The difference in growth consistency with respect to the automated method and radiologist

Table 3. Growth consistency results for automated method and radiologist boundary marking

Method	Average GC	Median GC	Range
Radiologist	3.78	3.12	0.05 - 13.60
Automated Method	2.46	1.87	0.3 - 6.46

had a p-value of 0.002, using the one-sided Wilcoxon test.

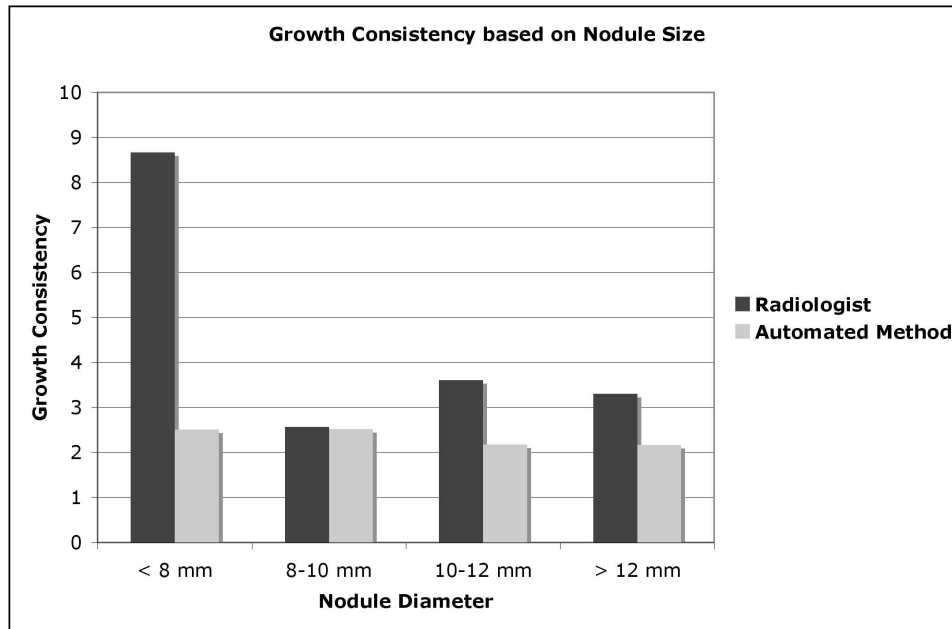


Figure 8. Average growth consistency with respect to nodule size. The automated method is more consistent than the radiologist by nearly 6 % in the lower size ranges.

The average size of the nodule across all three scans is plotted against the average growth consistency in figure 8. The smaller the nodule the more susceptible a volumetric measurement is to noise and other imaging artifacts. This impacts the accuracy in growth consistency and is evident in the nodule size range less than 8 mm. The radiologist boundary marking is considerably worse and indicates that automated segmentation methods could aid in the analysis of smaller-size nodules. As the nodule size increases, so does the accuracy in the GC calculation. For all size ranges, the automated method was more consistent than that of the radiologist.

The automated method is significantly more consistent between a GC of 2-3 percent. Across all the size ranges, the GC metric only changes by less than 0.5. The radiologist boundary marking method fluctuates from more than 8 percent difference in smaller size ranges to slightly above 3 percent for the larger size nodules. An 8 percent difference per month is a clearly significant change in volume over a period of one year.

From our observations, there was no clear issue in the lack of consistency from the radiologist markings. One possible explanation is in human measurement error and the difficulty in locating a consistent boundary for the nodule. In cases where our automated method was less consistent, errors in the segmentation of the nodule were the biggest challenge. Incomplete vessel removal from the nodule and excessive noise in the CT image were the two most significant issues with the segmentation method.

5. CONCLUSIONS

Measurement of lung nodule growth rate continues to be one of the most important features in determining the malignancy status. Accurate and consistent volumetric growth determination is a powerful tool for the

radiologist to better characterize the nature of the nodule. We have introduced a new method for segmentation of nonsolid nodules and examined its performance in measuring growth rates consistently. The results indicate that our automated method is more consistent at measuring volumetric growth than the radiologist 80 % of the time.

REFERENCES

1. K. Okada, D. Comaniciu, N. Dalal, and A. Krish, "Robust anisotropic gaussian fitting for volumetric characterization of pulmonary nodules in multislice CT," *IEEE Transactions on Medical Imaging* **24**, pp. 409–423, March 2005.
2. L. Zhang, M. Fang, D. P. Naidich, and C. L. Novak, "Consistent interactive segmentation of pulmonary ground glass nodules identified in ct studies," *Proceedings of SPIE* **5370**, pp. 1709 – 1717, 2004.
3. Y. Yoo, H. Shim, I. D. Yun, K. W. Lee, and S. U. Lee, "Segmentation of ground glass opacities by asymmetric multi-phase deformable model," *Proceedings of SPIE* **6144**, 2006.
4. R. Tachibana and S. Kido, "Automatic segmentation of pulmonary nodules on ct images by use of nci lung image database consortium," *Proceedings of SPIE* **6144**, 2006.
5. W. J. Kostis, A. P. Reeves, D. F. Yankelevitz, and C. I. Henschke, "Three-dimensional segmentation and growth-rate estimation of small pulmonary nodules in helical ct images," *IEEE Transactions on Medical Imaging* **22**, pp. 1259–1274, october 2003.
6. C. Tomasi and R. Manduchi, "Bilateral filtering for gray and color images," *Proceedings of the 1998 IEEE International Conference on Computer Vision* **6**, p. 839, 1998.
7. A. Reeves, A. Chan, D. Yankelevitz, C. Henschke, B. Kressler, and W. Kostis, "On measuring the change in size of pulmonary nodules," *IEEE Transactions on Medical Imaging* **25**, pp. 435–450, April 2006.
8. G. Agam and I. Dinstein, "Regulated morphological operations," *Pattern Recognition* **32**, pp. 947–971, 1999.